

Impact of Component Improvements within a Next Generation sCO₂ CSP Plant

Nicholas Chandler¹, Peter Schöttl²[\[https://orcid.org/0009-0003-1541-1355\]](https://orcid.org/0009-0003-1541-1355), Moritz Bitterling²[\[https://orcid.org/0009-0001-9158-7980\]](https://orcid.org/0009-0001-9158-7980), Gregor Bern²[\[https://orcid.org/0000-0002-5024-7699\]](https://orcid.org/0000-0002-5024-7699), and Thomas Fluri²

¹ Fraunhofer Institute for Solar Energy Systems ISE, Heidenhofstr. 2, 79110, Freiburg, Germany

² Fraunhofer Institute for Solar Energy Systems ISE, Heidenhofstr. 2, 79110, Freiburg, Germany

Abstract. Several component improvements within a next-generation CSP plant were investigated in the German-project, HeliogLOW, to determine their impact on the system performance. To accomplish this, multiple configurations of an upgraded CRS plant with four different components were parameterized and simulated using a transient simulation model. The four components introduced to the plant as upgrades are: a high temperature solid body receiver, an air curtain that reduces convection losses, a supercritical CO₂ power cycle that can operate at a range of temperatures, and an advanced heliostat field. With the result of multiple annual simulations under various operating conditions, configuration optima, performance sensitivity and specific component improvements were identified.

1. Introduction

The simultaneous upgrade of multiple components within a central receiver system (CRS) can have a compounding positive impact on the overall system performance. As such, the aim of the German-funded HeliogLOW project is to identify areas within CRS plants that can be further improved and then evaluate the resulting system performance improvements based on these component enhancements. Specifically, four different CRS components were evaluated. At the Fraunhofer ISE facilities in Freiburg, Germany, two laboratory experiments were performed: first, on a novel heat transfer medium consisting of a solid-body ceramic material which can operate at high temperatures and, second, on an air curtain, which minimizes the solar receiver's convective losses [1]. These experimental results were then integrated in a dynamic simulation model of a supercritical CO₂ (sCO₂) recompressed Brayton cycle, together with an optical assessment of an advanced heliostat design. The sizing of these components was parameterized to produce more than 900 unique CRS power plant configurations with different degrees of upgrades. From these results, three performance improvements were investigated:

1. What impact does a heliostat design have on the ability of a Solid Body Receiver (SoBoRec) to reach certain operational temperatures?
2. What are the key differences for a CRS system when the target sCO₂ turbine inlet temperature is raised from 650°C to 850°C, thereby increasing the thermal to electric conversion efficiency?
3. Can an air curtain that is attached to a receiver further increase the overall annual yield of the system?

2. Methodology

2.1 Simulation Model

Simulations of the next generation plant were performed using two Fraunhofer ISE in-house simulation tools, Raytrace3D and ColSim CSP. Raytrace3D is a software suite which calculates the flux distribution on absorber surfaces with high spatial resolution while taking into account optical effects [2]. ColSim CSP performs dynamic, annual yield assessments for solar thermal power plants and solar thermal process heat applications [3]. From these annual simulations, detailed, high resolution output for powerplant components such as the solar field, receiver, and power block can be evaluated.

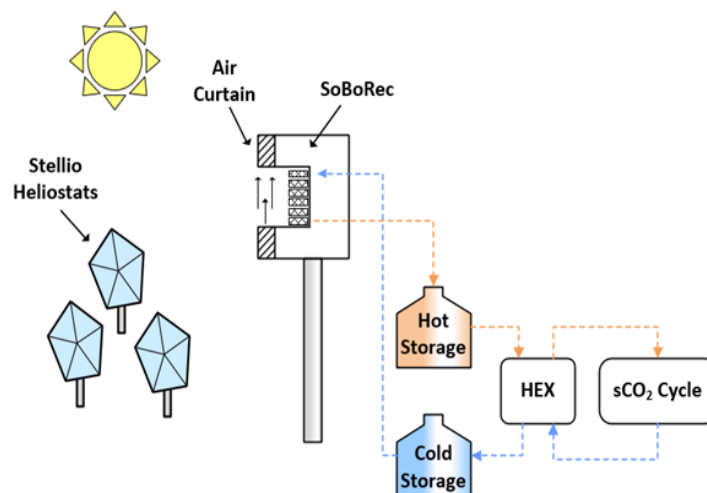


Figure 1. Diagram of the upgraded CRS system including the advanced heliostats, SoBoRec, sCO₂ Cycle, and air curtain.

The upgraded CRS plant with a direct thermal storage system (ref. Figure 1) consists of the following improvements: Solid Body Receiver (SoBoRec) system, solar receiver with a mounted air curtain, advanced heliostats, solid body thermal storage, a 12.9 MW_{e, gross} sCO₂ power cycle. Parasitic losses of the individual components such as heliostat tracking power, SoBo transportation and the air curtain were not considered to simplify the analysis of individual component performance improvements. Additionally, the thermal storage capacity of the system was chosen such that all the heat absorbed by the receiver could be utilized. In the following sections, the upgraded components are described in detail.

2.2 Solid Body Receiver (SoBoRec) System

A new solid body (SoBo) material was developed by Kraftblock GmbH and tested by Fraunhofer ISE under laboratory conditions. The purpose of this SoBo material is to utilize the non-corrosive, environmentally friendly qualities which ceramic material offers and then combine the solar absorber material, heat transfer fluid and storage material into a single component. This prototype material was tested at temperatures ranging from 500°C to 1350°C. However, for this paper, 500 – 1100°C is the chosen operational range of the SoBo material and a range of 800 – 1100°C for the receiver outlet temperature (Re_{C_T, out}). More information on the material properties of the prototype SoBo material is found in Table 1.

A cavity receiver system for the SoBoRec configuration is assumed with a square absorption area ranging from 40 – 120 m² and a SoBo thickness of 1 cm. It is assumed that a conveyor belt system transports the SoBo material between the receiver, thermal storage system, and heat exchanger in an adiabatic and isobaric process. In ColSim CSP, the absorbed radiation (with inputs from Raytrace3D), thermal radiation and convective losses, and other receiver performance values are calculated and printed at every timestep for further evaluation.

Table 1. Solid Body (SoBo) Material Properties.

Properties	Values
Density (ρ)	2010 kg·m ⁻³
Emissivity @1000°C (ϵ)	0.78 – 0.81
Solar weighted absorptance (α)	0.82
Specific heat capacity (c_p)	1270 J·kg ⁻¹ ·K ⁻¹
Thermal conductivity (λ)	0.71 W·m ⁻¹ ·K ⁻¹

2.3 Solar Receiver Mounted Air Curtain

Another aspect of the Helioglow project was to design and build a prototype air curtain which can be mounted in front of the SoBoRec. By blowing air as a clearly defined flow sheet in front of the receiver and thereby creating a thermal partition, the overall efficiency of the SoBoRec system is increased by reducing convective losses. A related SolarPACES 2022 paper describes the testing and performance of this air curtain prototype in detail [1]. The impact that the air curtain has on the heat absorption calculation within the ColSim CSP simulation model can be seen in Equations 1 and 2:

$$Q_{gain} = Q_{absorbed} - Q_{loss,refl} - Q_{loss,tr} - Q_{loss,cv} \quad (1)$$

where Q_{gain} is the total heat gain by the SoBoRec system, $Q_{absorbed}$ is the maximum potential heat absorbed available, $Q_{loss,refl}$ is the total reflected solar radiation loss, $Q_{loss,tr}$ is the total losses due to thermal radiation, and $Q_{loss,cv}$ is the total convective heat losses. The total convective are calculated in Equation 2:

$$Q_{loss,cv} = h \cdot A \cdot (T_{rec} - T_{amb}) \cdot (1 - C_{A.C.}) \quad (2)$$

where the convective heat losses, $Q_{loss,cv}$, are calculated by the multiplication of the convective heat transfer coefficient [4], h , which is calculated every timestep as a function of ambient temperature, receiver temperature and wind speed, the receiver area, A , the difference between the receiver temperature and the ambient temperature, $T_{rec} - T_{amb}$, and finally the air curtain improvement factor, $C_{A.C.}$. For this paper, a parametric range from 0% – 50% was used to study the effects of the air curtain improvement factor, $C_{A.C.}$. This range is in line with numerical simulations of air curtains as well as with the experimental observations, where a 30% improvement is considered conservative, and a 50% improvement is optimistic.

2.4 Advanced Heliostat Field

A reference solar field with a design thermal capacity of 50 MW_{th} and rectangular heliostats with an aperture area of 48.5 m² and a surface deviation of 1.5 mrad was designed for a reference receiver with an absorber area of 80 m². The heliostat field design used the MUEEN algorithm [5], which radially staggers the heliostat layout to prevent blocking. An extended version of the algorithm with additional optimization parameters (compression/stretching of the layout) was applied [6]. After the field aperture area was determined to be 84 875 m².

The Stellio[®] heliostat is an advanced heliostat developed by the Stellio Consortium [7], which features a pentagonal shape that reduces blocking and creates a low surface deviation (exact value confidential). The Stellio heliostat design was integrated in the Raytrace3D optical model. The pentagonal front surface is covered by several mirror facets, which are curved according to the slant range of the heliostat and form a reflective surface of 48.5 m².

While the field design algorithm with default parameters yields reasonably optimal layouts for rectangular heliostats, it is not intended originally for pentagonal heliostats. Thus, a two-

step optimization for three free compression/stretching parameters [6] of the extended MUEEN algorithm has been carried out, to achieve maximum annual, DNI-weighted, optical efficiency:

1. Assuming that the free parameters are weakly correlated, they are varied independently around their nominal value (unity, thus no compression/stretching) with a coarse resolution, in order to identify the approximate position of the global optimum.
2. Consequently, a fully factorial, coupled search on a finer grid in the vicinity of the identified location is carried out, to find the fine-tuned optimum.

It is found that the Stellio heliostats favor slightly increased row distances and slightly decreased distances of neighboring heliostats in the same row, compared to the rectangular heliostat layout. While the layout algorithm might not yield the optimum result for the Stellio heliostats, the optimized fields with both heliostat types achieve the same annual optical efficiency.

Based on the optimum field layout parameters, the reference aperture area and the rectangular heliostats, 25 optical profiles were created – using Raytrace3D and based on a *sky discretization* approach [8] – while varying the linear, combined slope/tracking deviation in a range from 0.9 to 2.5 mrad ([9], range should cover most state-of-the-art heliostats and is probably optimistic at the low end) and receiver area range of 40 m² to 120 m². By adjusting these two parameters, the radiation spillage in the system is mostly affected. Repercussions that change in these two parameters might have on the optimum field layout were neglected. In addition, 5 optical profiles for Stellio heliostats and varying receiver areas were derived.

2.5 sCO₂ Power Cycle and Heat Exchanger

Since the SoBo material can reach higher temperatures, a 12.9 MW_{el, gross} recompression supercritical CO₂ (sCO₂) cycle was introduced to the system as an upgrade to the power block. This power cycle, shown in Figure 2, was modeled after the findings in [10] and [11]. When incorporated into ColSim CSP, it was assumed that the sCO₂ model operates at a steady state under ideal conditions. To understand the effect of the high temperature performance of the receiver and the resulting required mass flow rates, a range of sCO₂ turbine inlet temperatures (sCO₂ T_{IT}) were considered for the sCO₂ cycle. With a range of 650°C to 850°C considered for the sCO₂ T_{IT}, the corresponding thermal to electric conversion efficiencies were determined to be between 50.0% and 54.9%, which are consistent with the results presented in [11].

To combine the sCO₂ cycle to the modelled system, a heat exchanger model was created which transfers the heat from the SoBo material to the CO₂. This fluidized bed heat exchanger was modelled in Modelica/Dymola. This modelling can determine the SoBoRec inlet temperature and SoBoRec mass flow rate based on the sCO₂ inlet, temperature, outlet temperature, mass flow rate and the Rec_{T, out}. For this study, it was assumed that the temperature difference (ΔT) between the sCO₂ T_{IT} and Rec_{T, out} is 150°C, 200°C, or 250°C.

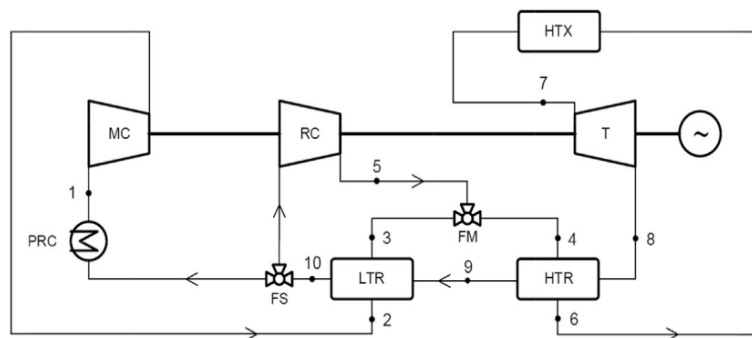


Figure 2. Layout of the modelled recompression sCO₂ cycle with turbine (T), main compressor (MC), recompression stage (RC), low temperature recuperator (LTR), high temperature recuperator (HTR), heat exchanger (HTX) flow merger (FM), flow splitter (FS), pre-cooling stage (PRC) [10].

2.6 Parameter Variation and Optimization

One key feature of ColSim CSP is its ability to run simulations simultaneously on multiple CPU cores, which is crucial when a large number of annual simulations are considered at high resolution. For the optimization process of this paper, a parametric approach was taken to include the parameter ranges considered in the previous section. Altogether, the combination of the different parameters shown in Table 2 led to more than 900 different simulation cases. Each simulation case consists of an annual simulation with a 120 second timestep. Additionally, the daily performance of each configuration was also considered for three summer days with very good DNI conditions ($900+ \text{ W/m}^2$).

Table 2. List of Component Parameterization Ranges

Component	Area of Parameterization	Parameter Range	Unit
Heliostat Field	Surface Deviation (σ)	0.9, 1.3, 1.7, 2.1, 2.5	mrad
Receiver	Receiver Area	40, 60, 80, 100, 120	m^2
	Outlet Temperatures ($\text{Re}_{\text{T, out}}$)	800 – 1100 (50 °C step)	°C
Air Curtain	Convective Loss Reduction	0, 50% (10% step)	%
sCO ₂ Cycle	Turbine Inlet Temperature (sCO ₂ TIT)	650 – 850 (50 °C step)	°C
Heat Exchanger	$\Delta T (\text{Re}_{\text{T, out}} - \text{sCO}_2 \text{ TIT})$	150, 200, 250	°C

3. Results and Discussion

3.1 Assessment on the improvements due to heliostat field surface deviation with increasing operating temperatures

The annual optical efficiencies of the rectangular heliostats and the Stellio heliostats can be seen in Figure 3, where the annual optical efficiencies begin to converge as the receiver area increases. This demonstrates the advanced performance of the Stellio field, which has an annual optical efficiency ranging from 61.9% – 68% and outperforms rectangular profiles with a slope deviation greater than 1.3 mrad. While the field design algorithm for the Stellio – as used herein – should be further improved, its advanced design improves the performance of the CRS system overall.

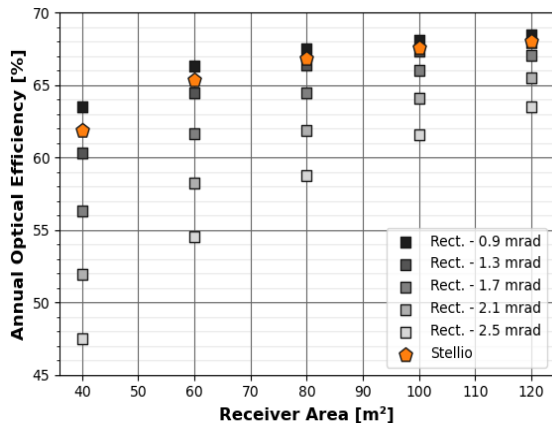


Figure 3. Annual optical efficiencies of the rectangular (varying surface quality) and Stellio heliostat fields as a function of receiver area.

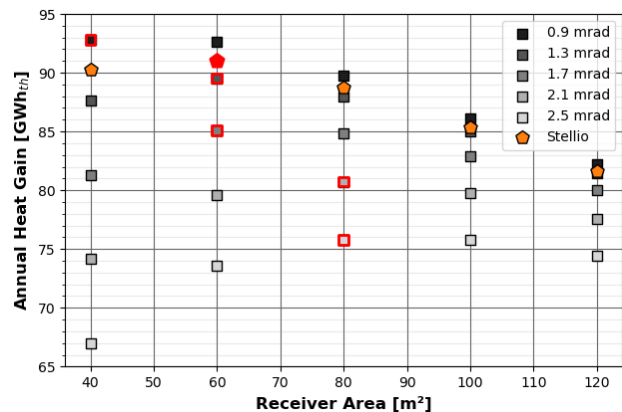


Figure 4. Annual heat gain of the rectangular (varying surface quality) and Stellio heliostat fields as a function of receiver area. Largest annual gain marked with red edge.

When the six different heliostat fields are integrated into a CRS plant with a receiver outlet temperature ($Re_{C_{T, out}}$) is 850°C and a $s\text{CO}_2_{TIT}$ of 700°C , the local optima can be determined for every slope deviation and receiver area. These optima represent the trade-off between spillage (increased for smaller receivers) and thermal losses (increased for larger receivers). In Figure 4, these optima, outlined in red, show the largest annual heat gain per heliostat type for a CRS plant. Overall, the annual heat gain of the optimized Stellio differs approximately $\pm 1.8\%$ for rectangular heliostats with slope deviation is less than 1.3 mrad, while the Stellio performs 7% to 20.4% better when a slope deviation is greater than 1.3 mrad.

In Figure 5, the heat profile shown over a sunny summer day for the aforementioned CRS plant configuration with a Stellio solar field is shown. In Figure 6, 33.8% to 38.1% of the total potential heat on the receiver, which exclude optical losses calculated in Raytrace3D, is converted to electricity. While the largest inefficiency of the system is the power block conversion inefficiency, the reflected solar radiation is the leading cause of heat lost and is calculated as a fixed percentage within the ColSim CSP simulation. To improve the performance, the SoBo could be darkened or coated to further reduce the reflective losses.

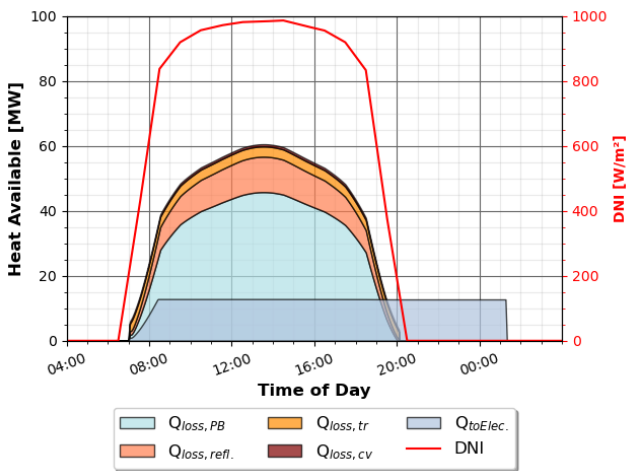


Figure 5. Example heat absorption and loss profile for a summer day.

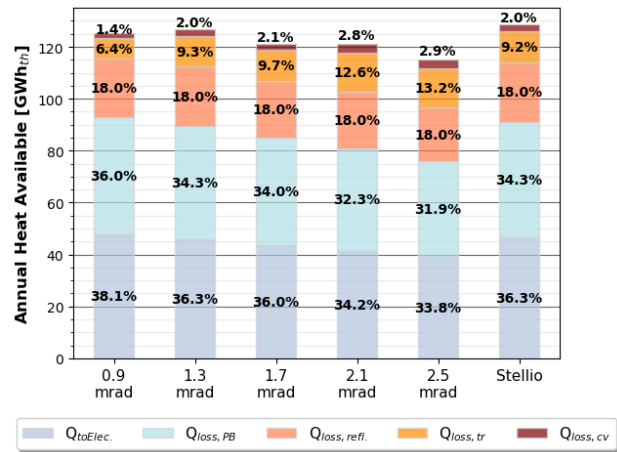


Figure 6. Annual heat loss breakdown for optima field layouts (red) from Figure 4.

The second largest contributor is the thermal radiation loss, which ranges from 6.4% for a smaller receiver area (40m^2) to 12.6 – 13.2% when the receiver area doubles in size. Lastly, the convective losses account for less than 3%, where the smaller area receivers have the smallest convective loss. Since the thermal radiation and convective losses calculations are receiver area dependent, a smaller receiver area would naturally result in smaller losses but, depending on the heliostat performance, could produce greater spillage. The balance between thermal losses and spillage is an important factor when in the optimization tool chain.

3.2 Assessment on the improvements due increased $s\text{CO}_2$ cycle temperature

When the $s\text{CO}_2_{TIT}$ is increased from 700°C to 800°C , there is an optimization tradeoff between the increase in the overall thermal-electric conversion efficiency and the increase in thermal losses due to a larger receiver area. In Figure 7, the optimized receiver areas are shown per heliostat type, where, as the receiver outlet temperature and heliostat surface error increases, the optimum receiver area decreases. Compared to the Figure 4 optimum areas which assumed a $Re_{C_{T, out}}$ of 800°C , the optimized receiver areas that increase by 20m^2 are the heliostat fields with a surface error of 0.9, 1.7 and 2.5 mrad. The optimized results could be further improved by widened receiver area parametric range and with more steps.

In Figure 8, the impact on the annual yield by varying the $Rec_{T, out}$ and sCO_2 TIT temperatures was evaluated for the optimized Stellio heliostat-receiver area configurations in . As the $Rec_{T, out}$ increases, so the yield increases between 1.6% and 1.8%. A peak in annual yield increase is seen for each ΔT considered. Two reasons for this peak can be attributed to the fact that the increase of $Rec_{T, out}$ does not necessarily increase the overall yield despite the sCO_2 cycle efficiency increase and that a smaller receiver area should be considered. As seen in Figure 8, a lower ΔT between the $Rec_{T, out}$ and sCO_2 TIT results in a higher the overall yield. However, the SoBo mass flow rate required to achieve this low ΔT could be physically improbable or economically unfeasible for the heat exchange design. Therefore, the heat exchanger sizing is a limiting factor in the optimization process.

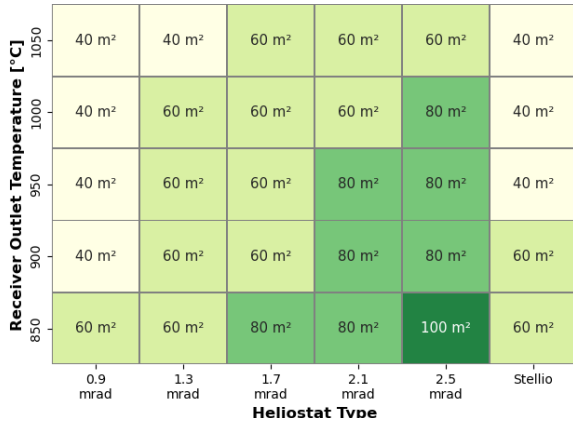


Figure 7. Optimized receiver areas as a function of receiver outlet temperature and Heliostat type.

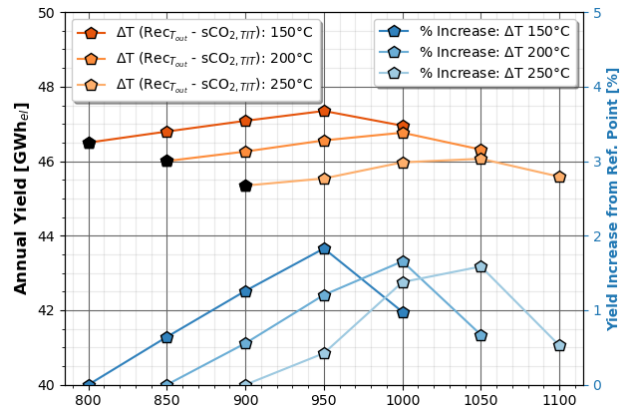


Figure 8. Annual yield, percent increase as a function of $Rec_{T, out}$ and sCO_2 TIT for the optimized Stellio field from Figure 7.

3.3 Assessment on the improvements due to the introduction of an Air Curtain

A parametric analysis was completed to introduce an air curtain for two different solar fields, rectangular heliostat with a 2.5 mrad surface error and the Stellio, that consider two receiver outlet temperatures. From the results determined in Figure 9 and Figure 10, the impact of the air curtain can be seen. For the Stellio heliostat configuration with a smaller receiver area, the air curtain increases the yield by 0.63% for a conservative $C_{A.C.}$ value and 1.12% to 1.36% for an optimistic value.

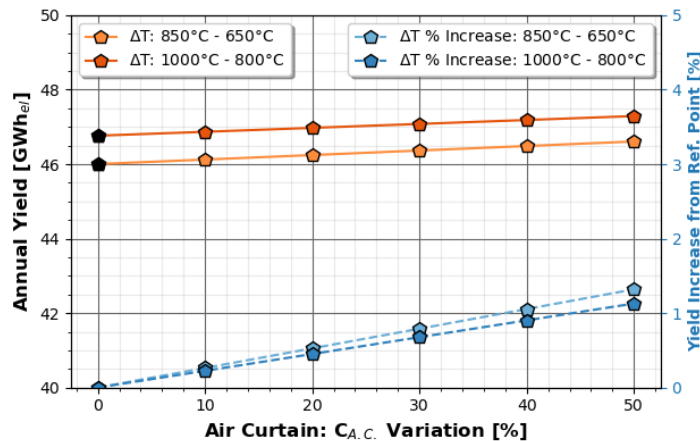


Figure 9. Annual yield as a function of air curtain efficiency for an optimized Stellio heliostat field.

For a rectangular heliostat with a poor surface quality, shown in Figure 10, the annual yield of the configuration is considerably less than the Stellio configuration. However, the impact of the air curtain is greater for this heliostat configuration by 1.47% to 1.56% for a conservative $C_{A.C.}$ value and 2.46% to 2.61% for an optimistic value. This larger improvement can be attributed to the larger receiver area needed for the low performance heliostats configuration. Areas of further investigation is the impact on the receiver area size when an air curtain is introduced, the parasitic load of an air curtain, and the economic costs to install such system.

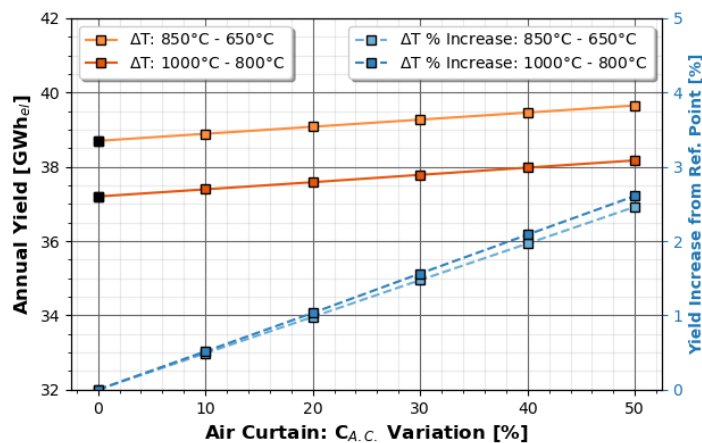


Figure 10. Annual yield as a function of air curtain efficiency for an optimized rectangular heliostat (2.5 mrad) field.

4. Conclusion

A CRS plant with a direct storage has been evaluated with the following upgrades: a high temperature solid body receiver, an air curtain which reduces receiver convection losses up to 50%, a supercritical CO_2 power cycle operating at a range of turbine inlet temperatures, and an advanced heliostat field. These different components were parameterized to produce over 900 CRS plant configurations and multiple annual simulations were executed, in order to measure the improvements of total heat gain and annual electricity generation. Optimum receiver area, receiver outlet temperature, and heliostat field configurations based upon set parameter conditions were also identified.

The advanced solar field increased the overall heat gain of the CRS system by 7% to 20.4% when rectangular with medium to high optical surface deviations are used. The receiver outlet temperature, the sCO_2 turbine inlet temperature and heat exchanger capabilities heavily impact the overall optimization of the system. Finally, the introduction of an air curtain was found to have a positive impact on the annual generation of configurations, especially those with large receiver areas. Further work might investigate the parasitic losses of the various upgraded components mentioned and a techno-economic evaluation of these components.

Data availability statement

Data and supplementary material will be provided upon request.

Author contributions

N. Chandler: Conceptualization, Software, Data curation, Formal analysis, Investigation, Methodology, Validation, Visualization, Writing – original draft. P. Schöttl: Methodology, Software, Validation, Writing – review & editing. M. Bitterling: Conceptualization, Data curation. G. Bern:

Conceptualization, Funding acquisition, Methodology, Project administration, Writing – review & editing. T. Fluri: Funding acquisition, Supervision, Writing – review & editing

Competing interests

The authors declare no competing interests.

Funding

The project, under which the work presented in this paper has been conducted, was funded by the German Federal Ministry for Economic Affairs and Climate Protection (BMWK) under code 0324174. The authors of this publication are responsible for its contents.

References

- [1] M. Bitterling *et al.*, "Experimental Test Setup of an Airwall to Reduce the Experimental Test Setup of an Airwall to Reduce the Convective Heat Loss in Solar Thermal Cavity Receivers," in *Proceedings of the SOLARPACES 2022: International Conference on Concentrating Solar Power and Chemical Energy Systems*, Albuquerque, NM (United States), 2022.
- [2] P. Schöttl, G. Bern, P. Nitz, F. Torres, and L. Graf, *Raytrace3D by Fraunhofer ISE: Accurate and Efficient Ray Tracing for Concentrator Optics*. [Online]. Available: <https://www.ise.fraunhofer.de/content/dam/ise/de/downloads/pdf/raytrace3d.pdf> (accessed: Apr. 30 2022).
- [3] C. Wittwer, "ColSim - Simulation von Regelungssystemen in aktiven solarthermischen Anlagen," Universität Karlsruhe, Fakultät für Architektur, 1999. [Online]. Available: http://www.opticontrol.ethz.ch/Lit/Witt_99_PhD-UnivKarlsruhe.pdf
- [4] D. L. Siebers and J. S. Kraabel, "Estimating Convective Energy Losses From Solar Central Receivers," Sandia National Laboratories SAND-84-8717, 1984.
- [5] F. Siala and M. Elayeb, "Mathematical formulation of a graphical method for a no-blocking heliostat field layout," *Renewable Energy*, vol. 23, no. 1, pp. 77–92, 2001, doi: [https://doi.org/10.1016/S0960-1481\(00\)00159-2](https://doi.org/10.1016/S0960-1481(00)00159-2).
- [6] E. Leonardi, L. Pisani, I. Les, A. Mutuberría, S. Rohani, and P. Schöttl, "Techno-Economic Heliostat Field Optimization: Comparative Analysis of Different Layouts," *Solar Energy*, vol. 180, pp. 601–607, 2019, doi: <https://doi.org/10.1016/j.solener.2019.01.053>.
- [7] M. Balz, V. Göcke, T. Keck, F. von Reeken, G. Weinrebe, and M. Wöhrbach, "Stellio – development, construction and testing of a smart heliostat," in *AIP Conference Proceedings 1734*, 2016, p. 20002. doi: <https://doi.org/10.1063/1.4949026>.
- [8] P. Schöttl, K. Ordóñez Moreno, D. W. van Rooyen, G. Bern, and P. Nitz, "Novel sky discretization method for optical annual assessment of solar tower plants," *Solar Energy*, vol. 138, pp. 36–46, 2016, doi: <https://doi.org/10.1016/j.solener.2016.08.049>.
- [9] G. Bern, P. Schöttl, D. W. van Rooyen, A. Heimsath, and P. Nitz, "Parallel in-situ measurement of heliostat aim points in central receiver systems by image processing methods," *Solar Energy*, vol. 180, pp. 648–663, 2019, doi: <https://doi.org/10.1016/j.solener.2019.01.051>.
- [10] M. A. Reyes-Belmonte, A. Sebastián, M. Romero, and J. González-Aguilar, "Optimization of a recompression supercritical carbon dioxide cycle for an innovative central receiver solar power plant," *Energy*, vol. 112, pp. 17–27, 2016, doi: <https://doi.org/10.1016/j.energy.2016.06.013>.

- [11] S. Trevisan, R. Guédez, and B. Laumert, "Thermo-economic optimization of an air driven supercritical CO₂ Brayton power cycle for concentrating solar power plant with packed bed thermal energy storage," *Solar Energy*, vol. 211, pp. 1373–1391, 2020, doi: <https://doi.org/10.1016/j.solener.2020.10.069>.